

Nucleon Size Independence of Hadronic Nucleus-Nucleus Cross Sections

Hao-jie Xu^{1,2,*}

¹*School of Science, Huzhou University, Huzhou, Zhejiang 313000, China*

²*Strong-Coupling Physics International Research Laboratory (SPiRL),
Huzhou University, Huzhou, Zhejiang 313000, China.*

Recent proposals to constrain the nucleon size using hadronic cross sections (σ_{AA}) conflict with collective flow data. I demonstrate this dependence is an artifact of “geometric inflation,” where smearing point-like nucleons unintentionally dilutes the nuclear surface. By implementing a self-consistent framework that preserves the global nuclear density, I show that σ_{AA} is essentially insensitive to the nucleon width. This establishes σ_{AA} as a robust probe of the nuclear surface rather than the sub-nucleon scale. Utilizing this property, I extract a neutron skin thickness for ^{208}Pb of $\Delta r_{\text{np}} \in [0, 0.24]$ fm, providing an unconventional way to constrain the nuclear symmetry energy using high-energy hadronic observables.

Introduction. Relativistic heavy-ion collisions create a deconfined state of Quantum Chromodynamics (QCD) matter known as the quark–gluon plasma (QGP) [1–4]. While relativistic hydrodynamics has been remarkably successful in describing the collective evolution of this hot and dense medium [5–20], the initial conditions of the collision remain a dominant source of uncertainty. Current phenomenological studies rely heavily on geometrical models that simplify the complex microscopic processes underlying thermalization [21–23].

In these frameworks, nucleon positions within the colliding nuclei are sampled stochastically from a Woods–Saxon distribution,

$$\rho^{\text{WS}}(r) = \frac{\rho_0}{1 + e^{(r-R)/a}}, \quad (1)$$

where R is the nuclear radius and a is the surface diffuseness. The normalization constant ρ_0 is typically adjusted dynamically in Monte Carlo simulations to match the mass number A . In the widely used TRENTo initial-state model [23], the probability of a nucleon–nucleon (NN) collision is determined by an effective parton–parton cross section, σ_{gg} , and a Gaussian nucleon width, w . The inelastic NN cross section, σ_{NN} , is related to these parameters via the integral of the interaction probability:

$$\sigma_{\text{NN}} = \int d^2\mathbf{b} [1 - \exp(-\sigma_{\text{gg}} T_{pp}(\mathbf{b}))], \quad (2)$$

where the nucleon–nucleon overlap function is $T_{pp}(\mathbf{b}) = \exp(-b^2/4w^2)/(4\pi w^2)$. For $^{208}\text{Pb}+^{208}\text{Pb}$ collisions at $\sqrt{s_{\text{NN}}} = 5.02$ TeV, σ_{NN} is fixed to 70 mb. Consequently, σ_{gg} becomes dependent on the width w .

A critical consequence of this ansatz is that the hadronic nucleus–nucleus cross section, σ_{AA} , acquires an explicit dependence on the nucleon size w . This dependence has recently been proposed as an observable to constrain the effective nucleon size, yielding $w \approx 0.4\text{--}0.5$ fm when compared to ALICE measurements ($\sigma_{AA} = 7.67 \pm 0.25$ b) [24, 25]. This small width is consistent with earlier Bayesian analyses [12] and the proton charge radius ($r_{\text{ch,p}} \approx 0.84$ fm) [26]. However, it stands in tension with recent global Bayesian analyses that

favor significantly larger values, $w \approx 1$ fm [13–15]. Resolving this discrepancy is crucial for the precision of initial-state modeling [24, 27, 28].

In this Letter, I demonstrate that the sensitivity of σ_{AA} to w is an artifact of the standard modeling procedure and can be eliminated by ensuring a self-consistent nuclear density. I further propose utilizing the resulting w -independent σ_{AA} as a precision probe to constrain the neutron skin thickness of ^{208}Pb .

Self-consistent nuclear density. The apparent dependence of σ_{AA} on w arises from a mathematical inconsistency between the point-like Monte Carlo sampling of nucleon positions and their subsequent modeling with finite-width Gaussian profiles. When a distribution of point-like centers is convolved with Gaussian kernels of width w , the resulting matter profile is inherently broader than the original sampling distribution. Consequently, starting from a fixed Woods–Saxon distribution for the centers and increasing w unintentionally distorts the global nuclear geometry. This creates a “geometric inflation” (illustrated in Fig. 1) where changes in nucleon size mimic changes in nuclear density.

This artifact is well-documented in other fields, such as quantum molecular dynamics for intermediate-energy reactions [29–31] and the extraction of point-proton densities from charge distributions [32–34]. While this inflation is rigorously accounted for in nuclear structure physics, it has been largely overlooked in relativistic heavy-ion simulations.

To recover the target Woods–Saxon density $\rho^{\text{WS}}(\mathbf{r})$, the sampling distribution for nucleon centers, $f(\boldsymbol{\xi})$, must be modified as a function of w . The relationship between the center distribution and the final density is governed by the convolution:

$$\rho(\mathbf{r}; w) = \int d^3\xi f(\boldsymbol{\xi}) K_p(\mathbf{r}, \boldsymbol{\xi}). \quad (3)$$

For the Gaussian kernel $K_p(\mathbf{r}, \boldsymbol{\xi}) = \exp\left(-\frac{(\mathbf{r}-\boldsymbol{\xi})^2}{2w^2}\right)/(2\pi w^2)^{3/2}$, this defines a three-dimensional Weierstrass transform. To ensure the physical density $\rho(\mathbf{r}; w)$ remains invariant and matches the target $\rho^{\text{WS}}(\mathbf{r})$, the sampling distribution $f(\boldsymbol{\xi})$ must be treated as the mathematical antecedent, resolved via the inverse transform (deconvolution).

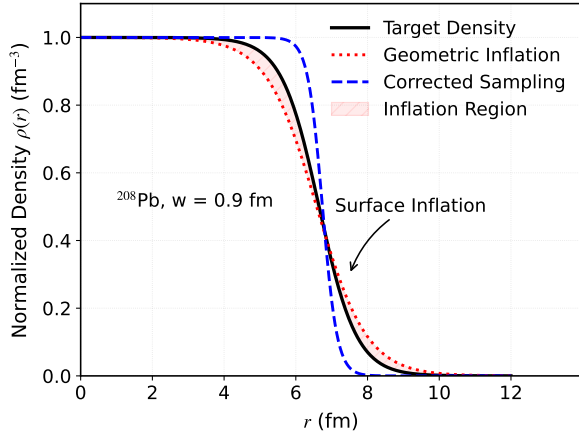


FIG. 1. (Color online). Illustration of geometric inflation. The target Woods–Saxon distribution is compared with the inflated density from uncorrected sampling for $w = 0.9$ fm. The corrected sampling distribution, obtained via inverse transform, ensures the physical density matches the target after convolution.

While formally inverting Eq. (3) is possible, it is numerically non-trivial. I therefore adopt a robust analytical approach by assuming $f(\xi)$ follows a Woods–Saxon form with modified parameters $(\tilde{\rho}_0, \tilde{R}, \tilde{a})$ [32–35]. For a given w , these modified parameters are constrained by matching the first three radial moments of the convolved density to the target distribution:

$$\langle \rho(r; w) \rangle = \langle \rho^{\text{WS}}(r) \rangle, \quad (4)$$

$$\langle r\rho(r; w) \rangle = \langle r\rho^{\text{WS}}(r) \rangle, \quad (5)$$

$$\langle r^2\rho(r; w) \rangle = \langle r^2\rho^{\text{WS}}(r) \rangle, \quad (6)$$

where $\langle r^n g \rangle \equiv \int r^n g(\mathbf{r}) d^3r / \int g(\mathbf{r}) d^3r$.

Figure 2 illustrates the evolution of \tilde{R} and \tilde{a} required to maintain the physical density of ^{208}Pb ($R = 6.647$ fm, $a = 0.523$ fm for charge distribution [36]) as w varies. As w increases, the sampling diffuseness \tilde{a} must decrease sharply to counteract the surface broadening caused by the Gaussian convolution. Simultaneously, \tilde{R} undergoes a slight adjustment.

Using the approximation $\tilde{\rho}_0 \equiv \rho_0$, the parameters can be estimated analytically from Eqs. (4) and (6) [33, 34]:

$$\begin{aligned} \tilde{R} &\approx R + w^2 \frac{15R}{15R^2 + 7\pi^2 a^2}, \\ \tilde{a} &= \sqrt{a^2 - \frac{\tilde{R}^3 - R^3}{\pi^2 \tilde{R}}}. \end{aligned} \quad (7)$$

Equation (7) captures the essential behavior: $\tilde{a}^2 \approx a^2 - 3w^2/\pi^2$, highlighting the subtractive correction to the diffuseness. A physical upper bound of $w \approx 0.9$ fm exists for ^{208}Pb ; beyond this, \tilde{a} would become unphysical, consistent with liquid-drop model expectations ($w \approx 1.83a$) [37]. This approximation, yielding $\tilde{R} = 6.682$ fm and $\tilde{a} = 0.447$ fm, is commonly used for the point-proton distribution [22, 24, 32, 38]. However, this requires $w = 0.494$ fm ($r_p = 0.856$ fm); varying

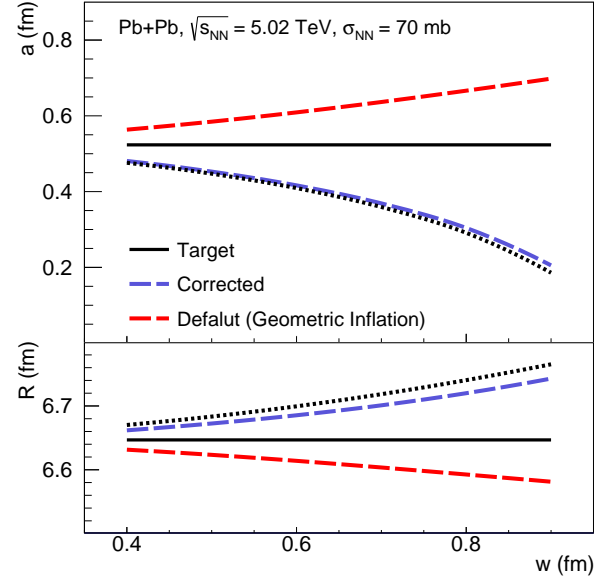


FIG. 2. (Color online). The (effective) Woods–Saxon parameters for the target density (R, a), the inflated density ($R_{\text{eff}}, a_{\text{eff}}$, constrained by Eqs. (4)–(6)), and the corrected density (\tilde{R}, \tilde{a}). The black dashed curves represent the analytical approximation in Eq. (7).

w in the usual way for mass density creates tension between nuclear and sub-nuclear structure.

Implementing these corrected sampling parameters yields the central result of this Letter: $\sigma_{\text{AA}} \approx 7.43$ b, which is essentially independent of the nucleon width w (blue solid curve, Fig. 3). This stands in stark contrast to the strong dependence reported in Ref. [24] (red dashed curve). The previously observed sensitivity of σ_{AA} to w is therefore confirmed as an artifact of geometric inflation. Once corrected, σ_{AA} decouples from the nucleon size, resolving the tension with Bayesian parameter estimations.

Probing the neutron skin thickness. Having established that σ_{AA} is insensitive to the nucleon width w when the nuclear density is treated self-consistently, I now examine its robustness against other model parameters. Similar to Ref. [24], I find that σ_{AA} is largely unaffected by the minimum inter-nucleon distance d_{min} and that its variation with the inelastic nucleon–nucleon cross section σ_{NN} is negligible within current experimental uncertainties.

Furthermore, I argue that the centrality normalization factor—identified in Ref. [24] as a dominant source of uncertainty—should not be treated as a free parameter for σ_{AA} calculations. Experimental measurements, such as those by ALICE [25], already incorporate efficiency corrections to report the total inelastic cross section. Therefore, the theoretical calculation should simply sum all generated interaction events. Variations arising from different model kernels should be treated as systematic theoretical uncertainties rather than tunable normalization factors.

With the influence of these parameters thus constrained or eliminated, σ_{AA} emerges as a precision probe of the underlying

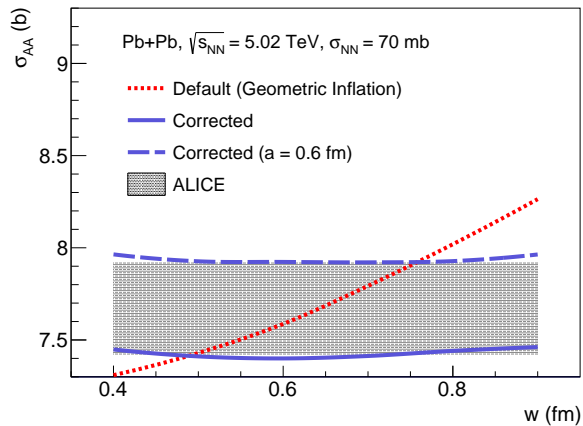


FIG. 3. (Color online). σ_{AA} for $^{208}\text{Pb}+^{208}\text{Pb}$ collisions at $\sqrt{s_{NN}} = 5.02$ TeV, computed with the default Woods–Saxon parameters (red dashed curve) and with the Gaussian-kernel-corrected Woods–Saxon parameters (blue solid curve), compared with the horizontal band of ALICE measurements [25]. The blue dashed curve shows the effect of increasing the diffuseness to $a = 0.6$ fm.

nuclear density profile. Utilizing a Woods-Saxon parameterization anchored to the experimental charge distribution of ^{208}Pb , I describe the total mass density by assuming protons and neutrons share a common effective size w . Assuming identical proton and neutron distributions ($\Delta r_{np} = 0$), the calculated σ_{AA} aligns with the lower bound of the ALICE measurement ($7.67 - 0.25$ b) [25]. Here, the point-proton radius is derived from the charge radius R_{ch} via $R_{point}^2 = R_{ch}^2 - r_{ch,p}^2$, with $r_{ch,p} = 0.8414$ fm [26].

To reconcile the calculation with the upper experimental bound ($\sigma_{AA} \approx 7.92$ b), the mass (point-neutron) distribution must be extended. I find that σ_{AA} exhibits significantly higher sensitivity to the surface diffuseness a than to the half-radius R . While the data can be matched by increasing R to 6.95 fm (at fixed $a = 0.523$ fm), this implies a physically implausible skin thickness of $\Delta r_{np} = 0.359$ fm. In contrast, increasing the diffuseness to $a = 0.60$ fm (at fixed $R = 6.647$ fm) reproduces the data with a moderate skin of $\Delta r_{np} = 0.176$ fm (Fig. 3). This preference for a diffuseness-driven “halo-type” extension over a radius-driven “skin-type” one is consistent with density functional theory and previous experimental results [35, 39, 40].

In this framework, I employ a single Woods-Saxon profile for the total mass density; modeling protons and neutrons with distinct profiles would result in a total density that deviates from the standard Woods-Saxon form, requiring a numerical solution to Eq. (3). Notably, the extracted Δr_{np} retains a dependence on the physical choice of w , which dictates the spatial volume individual protons contribute to the mass density. If w is identified with the proton charge radius, the ALICE data imply $\Delta r_{np} \in [0, 0.176]$ fm. However, if a smaller width is adopted—such as the gluonic radius $w \approx 0.5$ fm suggested by J/ψ photoproduction [41]—the individual nucleons occupy less volume. To preserve the total mass density constrained

by σ_{AA} , the neutron distribution must extend further outward, yielding $\Delta r_{np} \in [0.069, 0.243]$ fm.

Applying the established linear relation $\Delta r_{np} \approx 0.101 + 0.00147L$ [42], these ranges constrain the nuclear symmetry energy slope to $L \in [-69, 97]$ MeV. This result is consistent with global constraints [43, 44] and compatible with the lower bound of the PREX-II measurement ($L = 105 \pm 37$ MeV) [45, 46]. More precise measurements of σ_{AA} are required to further refine these unconventional constraints on the nuclear equation of state.

Uncertainties from nucleon diffuseness. The preceding discussion focused on the Gaussian ansatz; however, the nucleon thickness function $T_{pp}(b)$ depends on the specific form factor assumed for the nucleon. A generalized expression for the thickness function is given by

$$T_{pp}(b) = \frac{\kappa}{4\pi\zeta^2} (b/\zeta)^\gamma K_\gamma(b/\zeta), \quad (8)$$

where K_γ is the modified Bessel function of the second kind, and $\kappa = 2^{(1-\gamma)}/\Gamma(\gamma+1)$ is a normalization constant ensuring $\int d^2\mathbf{b} T_{pp}(b) = 1$. For $\gamma = 1$ and $\gamma = 3$, Eq. (8) reproduces the monopole and dipole form factors $F(q)$ via a Fourier-Bessel transform [47–52], corresponding to Yukawa-like and exponential nucleon profiles. The Gaussian limit is recovered as $\gamma \rightarrow \infty$ with the scaling $w \equiv \sqrt{\gamma+1}\zeta$. The properties of this general nucleon–nucleon thickness function are summarized in Table I.

Figure 4 compares $T_{pp}(b)$ at fixed $r_p = r_{ch,p}$ and the effective parton–parton cross section σ_{gg} for the three kernels with $\sigma_{NN} = 70$ mb (black dashed line). The dipole and monopole forms have softer tails than the Gaussian, and σ_{gg} shows similar trends for all three. To maintain self-consistency, the corrected sampling parameters \tilde{R} and \tilde{a} were obtained by inserting the appropriate kernel into the convolution in Eq. (3). For fixed $r_p = r_{ch,p}$, this gives $\tilde{R} \approx 6.672$ fm and $\tilde{a} \approx 0.456$ fm (with \tilde{a} decreasing slightly as γ decreases) for all kernels. Notably, even with the global density fixed to the target mass distribution, the calculated cross sections exhibit non-negligible variation: $\sigma_{AA} = 7.41$ b (Gaussian), 7.55 b (Dipole), and 7.60 b (Monopole). This reveals that while the *size* dependence (the geometric inflation artifact) is eliminated by the inverse transform, the *shape* of the nucleon profile—specifically its diffuseness—remains a source of physical uncertainty. A softer nucleon profile (smaller γ , longer tail) increases σ_{AA} , mimicking a more diffuse nuclear surface. This dependence is not an artifact of the inverse transform approximation: input densities from a numerical, matrix-based convolution agree with the moment-matching results obtained here.¹

¹ I take the convoluted Woods–Saxon density ($\tilde{R} = 6.672$ fm, $\tilde{a} = 0.456$ fm) with a Gaussian kernel ($r_p = r_{ch,p}$) as the target mass density, and compute the monopole and dipole input densities by matrix-based convolution to reproduce this target. The σ_{AA} from these numerical densities agrees with the simple Woods–Saxon approximation.

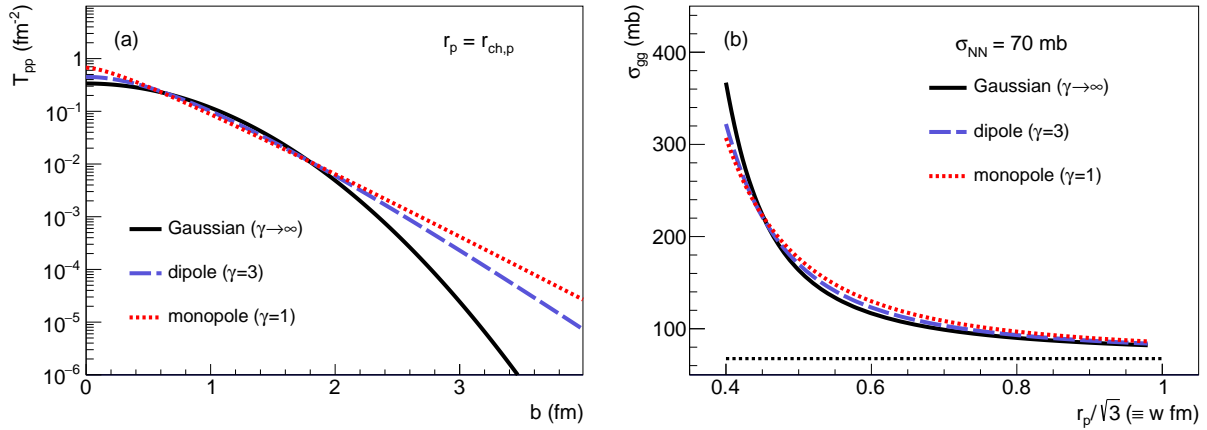


FIG. 4. (Color online). (a) Thickness function $T_{pp}(b)$ vs impact parameter for different nucleon form-factor approximations with nucleon radius $r_p = r_{ch,p}$; (b) corresponding effective parton–parton cross section vs nucleon size. The γ parameters relate to the general thickness function formula given in Eq. (8).

TABLE I. Properties of the nucleon–nucleon thickness function $T_{pp}(b)$, single nucleon form factor, nucleon density, and root-mean-square radius for different shape parameters γ . The scale parameters are ζ (for finite γ) and $w = \zeta\sqrt{\gamma+1}$ (for the Gaussian limit). The normalization constants are $\kappa = 2^{1-\gamma}/\Gamma(\gamma+1)$ and $\nu = (1+\gamma)/2$.

Case	Thickness function $T_{pp}(b)$	Form factor $F(q)$	Nucleon density $\rho(r)$	RMS radius r_p
General γ	$\frac{\kappa}{4\pi\zeta^2} \left(\frac{b}{\zeta}\right)^\gamma K_\gamma\left(\frac{b}{\zeta}\right)$	$\frac{1}{(1+q^2\zeta^2)^\nu}$	$\frac{1}{(2\pi)^{3/2}\zeta^3} \frac{2^{1-\nu}}{\Gamma(\nu)} \left(\frac{r}{\zeta}\right)^{\nu-3/2} K_{\nu-3/2}\left(\frac{r}{\zeta}\right)$	$\sqrt{3(1+\gamma)}\zeta$
$\gamma = 1$ (monopole)	$\frac{1}{4\pi\zeta^2} \frac{b}{\zeta} K_1\left(\frac{b}{\zeta}\right)$	$\frac{1}{1+q^2\zeta^2}$	$\frac{1}{4\pi r\zeta^2} e^{-r/\zeta}$	$\sqrt{6}\zeta$
$\gamma = 3$ (dipole)	$\frac{1}{96\pi\zeta^2} \left(\frac{b}{\zeta}\right)^3 K_3\left(\frac{b}{\zeta}\right)$	$\frac{1}{(1+q^2\zeta^2)^2}$	$\frac{1}{8\pi\zeta^3} e^{-r/\zeta}$	$2\sqrt{3}\zeta$
$\gamma \rightarrow \infty$ (Gaussian)	$\frac{1}{4\pi w^2} \exp\left(-\frac{b^2}{4w^2}\right)$	$\exp\left(-\frac{q^2 w^2}{2}\right)$	$\frac{1}{(2\pi)^{3/2} w^3} \exp\left(-\frac{r^2}{2w^2}\right)$	$\sqrt{3}w$

Thus, σ_{AA} is not strictly independent of the nucleon model; rather, it is robust against the width parameter w but sensitive to the functional form (diffuseness) of the density kernel. This ~ 0.2 b systematic uncertainty is comparable to current experimental errors. Consequently, precise extraction of the neutron skin from σ_{AA} requires better constraints on the nucleon’s gluonic shape, which may be provided by future electron–ion collider data [53].

Discussions. The resolution of the geometric inflation artifact clarifies the tension in the extracted nucleon size. Bayesian analyses of flow data, which favor $w \sim 1$ fm [13–15], typically vary w without the self-consistent density correction. In such a framework, increasing w not only modifies the sub-nucleonic profile but also—through geometric inflation—systematically dilates the effective nuclear matter distribution. The Bayesian preference for a larger w may therefore reflect an empirical compensation for an underlying nuclear density that is effectively too compact, rather than a genuine physical enlargement of the nucleon. A comprehensive picture must also account for initial-state fluctuations, which are intertwined with both nuclear geometry and sub-nucleonic structure [54].

These findings have broad implications for phenomenological frameworks [23, 52, 55], especially those where point-like sampling and specific nucleon kernels inadvertently enlarge the nuclear volume. For future precision studies, I propose two strategies: (1) fix w to a known nuclear-structure value (e.g., the proton charge radius) and vary only the Woods–Saxon parameters to match the physical density; or (2) explicitly separate nuclear geometry from sub-nucleonic smearing via the self-consistent method shown here. The second approach removes the coupling between w and global density, providing a clear route to resolving the apparent w puzzle in collective flow.

While I assumed a constant nucleon size, the nucleon profile in a nucleus may vary from the core to the surface [56–59]. Because nucleon profiles are central to nuclear structure and heavy-ion simulations, a self-consistent treatment that preserves the target nuclear density under convolution is essential for next-generation precision studies of nuclear and sub-nucleon structure. With a spherical nucleon profile, geometric inflation has little impact on nuclear deformation. A promising direction is to study how an anisotropic kernel affects nuclear

deformation and flow observables in relativistic heavy ion and p+p/p+Pb collisions [60, 61].

In summary, I have demonstrated that the reported sensitivity of σ_{AA} to nucleon size is a modeling artifact caused by non-conserved nuclear density. By resolving this through an effective inverse Weierstrass transform, σ_{AA} becomes a robust observable for nuclear geometry rather than sub-nucleonic structure. Although experimental uncertainties remain significant, this framework provides an unconventional way to constrain the nuclear symmetry energy slope L via high-energy collisions. These findings establish that density-consistent initial-state modeling is essential for disentangling QGP transport properties from the underlying nuclear structure.

Acknowledgments. The author thanks Dandan Zhang, Yingxun Zhang, and Qing Zhao for interesting discussions. This work is supported in part by the National Natural Science Foundation of China under Grants No. 12275082.

* haojiexu@zjhu.edu.cn

- [1] K. Adcox et al. (PHENIX Collaboration), Formation of dense partonic matter in relativistic nucleus-nucleus collisions at RHIC: Experimental evaluation by the PHENIX collaboration, *Nucl.Phys.* **A757**, 184 (2005), arXiv:nucl-ex/0410003 [nucl-ex].
- [2] J. Adams et al. (STAR Collaboration), Experimental and theoretical challenges in the search for the quark gluon plasma: The STAR Collaboration's critical assessment of the evidence from RHIC collisions, *Nucl.Phys.* **A757**, 102 (2005), arXiv:nucl-ex/0501009 [nucl-ex].
- [3] K. Aamodt et al. (ALICE), Elliptic flow of charged particles in Pb-Pb collisions at 2.76 TeV, *Phys. Rev. Lett.* **105**, 252302 (2010), arXiv:1011.3914 [nucl-ex].
- [4] E. Shuryak, Physics of Strongly coupled Quark-Gluon Plasma, *Prog.Part.Nucl.Phys.* **62**, 48 (2009), arXiv:0807.3033 [hep-ph].
- [5] J.-Y. Ollitrault, Anisotropy as a signature of transverse collective flow, *Phys.Rev.* **D46**, 229 (1992).
- [6] P. Kovtun, D. Son, and A. Starinets, Viscosity in strongly interacting quantum field theories from black hole physics, *Phys.Rev.Lett.* **94**, 111601 (2005), arXiv:hep-th/0405231 [hep-th].
- [7] P. Romatschke and U. Romatschke, Viscosity Information from Relativistic Nuclear Collisions: How Perfect is the Fluid Observed at RHIC?, *Phys.Rev.Lett.* **99**, 172301 (2007), arXiv:0706.1522 [nucl-th].
- [8] C. Shen, Z. Qiu, H. Song, J. Bernhard, S. Bass, and U. Heinz, The iEBE-VISHNU code package for relativistic heavy-ion collisions, *Comput. Phys. Commun.* **199**, 61 (2016), arXiv:1409.8164 [nucl-th].
- [9] H.-j. Xu, Z. Li, and H. Song, High-order flow harmonics of identified hadrons in 2.76A TeV Pb + Pb collisions, *Phys. Rev.* **C93**, 064905 (2016), arXiv:1602.02029 [nucl-th].
- [10] W. Zhao, H.-j. Xu, and H. Song, Collective flow in 2.76 A TeV and 5.02 A TeV Pb+Pb collisions, *Eur. Phys. J. C* **77**, 645 (2017), arXiv:1703.10792 [nucl-th].
- [11] B. Schenke, C. Shen, and P. Tribedy, Running the gamut of high energy nuclear collisions, *Phys. Rev. C* **102**, 044905 (2020), arXiv:2005.14682 [nucl-th].
- [12] J. E. Bernhard, J. S. Moreland, S. A. Bass, J. Liu, and U. Heinz, Applying Bayesian parameter estimation to relativistic heavy-ion collisions: simultaneous characterization of the initial state and quark-gluon plasma medium, *Phys. Rev. C* **94**, 024907 (2016), arXiv:1605.03954 [nucl-th].
- [13] J. E. Bernhard, J. S. Moreland, and S. A. Bass, Bayesian estimation of the specific shear and bulk viscosity of quark-gluon plasma, *Nature Phys.* **15**, 1113 (2019).
- [14] D. Everett et al. (JETSCAPE), Multisystem Bayesian constraints on the transport coefficients of QCD matter, *Phys. Rev. C* **103**, 054904 (2021), arXiv:2011.01430 [hep-ph].
- [15] G. Nijs, W. van der Schee, U. Gürsoy, and R. Snellings, Bayesian analysis of heavy ion collisions with the heavy ion computational framework Trajectum, *Phys. Rev. C* **103**, 054909 (2021), arXiv:2010.15134 [nucl-th].
- [16] J.-f. Wang, H.-j. Xu, and F.-Q. Wang, Impact of initial fluctuations and nuclear deformations in isobar collisions, *Nucl. Sci. Tech.* **35**, 108 (2024), arXiv:2305.17114 [nucl-th].
- [17] C. Gale, S. Jeon, and B. Schenke, Hydrodynamic Modeling of Heavy-Ion Collisions, *Int. J. Mod. Phys. A* **28**, 1340011 (2013), arXiv:1301.5893 [nucl-th].
- [18] R. Derradi de Souza, T. Koide, and T. Kodama, Hydrodynamic Approaches in Relativistic Heavy Ion Reactions, *Prog. Part. Nucl. Phys.* **86**, 35 (2016), arXiv:1506.03863 [nucl-th].
- [19] J. Noronha-Hostler, L. Yan, F. G. Gardim, and J.-Y. Ollitrault, Linear and cubic response to the initial eccentricity in heavy-ion collisions, *Phys. Rev. C* **93**, 014909 (2016), arXiv:1511.03896 [nucl-th].
- [20] H. Song, Y. Zhou, and K. Gajdosova, Collective flow and hydrodynamics in large and small systems at the LHC, *Nucl. Sci. Tech.* **28**, 99 (2017), arXiv:1703.00670 [nucl-th].
- [21] M. L. Miller, K. Reygers, S. J. Sanders, and P. Steinberg, Glauber modeling in high energy nuclear collisions, *Ann. Rev. Nucl. Part. Sci.* **57**, 205 (2007), arXiv:nucl-ex/0701025.
- [22] C. Loizides, Glauber modeling of high-energy nuclear collisions at the subnucleon level, *Phys. Rev. C* **94**, 024914 (2016), arXiv:1603.07375 [nucl-ex].
- [23] J. S. Moreland, J. E. Bernhard, and S. A. Bass, Alternative ansatz to wounded nucleon and binary collision scaling in high-energy nuclear collisions, *Phys. Rev. C* **92**, 011901 (2015), arXiv:1412.4708 [nucl-th].
- [24] G. Nijs and W. van der Schee, Hadronic Nucleus-Nucleus Cross Section and the Nucleon Size, *Phys. Rev. Lett.* **129**, 232301 (2022), arXiv:2206.13522 [nucl-th].
- [25] S. Acharya et al. (ALICE), ALICE luminosity determination for Pb-Pb collisions at $\sqrt{s_{NN}} = 5.02$ TeV, *JINST* **19** (02), P02039, arXiv:2204.10148 [nucl-ex].
- [26] E. Tiesinga, P. J. Mohr, D. B. Newell, and B. N. Taylor, CODATA recommended values of the fundamental physical constants: 2018*, *Rev. Mod. Phys.* **93**, 025010 (2021).
- [27] G. Giacalone, B. Schenke, and C. Shen, Constraining the Nucleon Size with Relativistic Nuclear Collisions, *Phys. Rev. Lett.* **128**, 042301 (2022), arXiv:2111.02908 [nucl-th].
- [28] H.-C. Wang, S.-J. Li, J. Xu, and Z.-Z. Ren, Disentangling effects of nucleon size and nucleus structure in relativistic heavy-ion collisions, *Phys. Lett. B* **866**, 139516 (2025), arXiv:2504.19082 [nucl-th].
- [29] J. Xu et al. (TMEP), Understanding transport simulations of heavy-ion collisions at 100A and 400A MeV: Comparison of heavy-ion transport codes under controlled conditions, *Phys. Rev. C* **93**, 044609 (2016), arXiv:1603.08149 [nucl-th].
- [30] J. Yang, Y. Zhang, N. Wang, and Z. Li, Influence of the treatment of initialization and mean-field potential on the neutron to proton yield ratios, *Phys. Rev. C* **104**, 024605 (2021), arXiv:2103.13132 [nucl-th].
- [31] X. Xiang, M. Nan, P. Li, Y. Wang, L. Liu, and Q. Li, Improved

- initial colliding nuclei density profile method for QMD-type transport models, (2025), [arXiv:2509.19089 \[nucl-th\]](#).
- [32] B. Klos et al., Neutron density distributions from antiprotonic Pb-208 and Bi-209 atoms, *Phys. Rev. C* **76**, 014311 (2007), [arXiv:nucl-ex/0702016](#).
- [33] L. L. Salcedo, E. Oset, M. J. Vicente-Vacas, and C. Garcia-Recio, Computer Simulation of Inclusive Pion Nuclear Reactions, *Nucl. Phys. A* **484**, 557 (1988).
- [34] E. Oset, P. Fernandez de Cordoba, L. L. Salcedo, and R. Brockmann, Decay Modes of Σ and Λ Hypernuclei, *Phys. Rept.* **188**, 79 (1990).
- [35] H.-j. Xu, H. Li, X. Wang, C. Shen, and F. Wang, Determine the neutron skin type by relativistic isobaric collisions, *Phys. Lett. B* **819**, 136453 (2021), [arXiv:2103.05595 \[nucl-th\]](#).
- [36] G. Fricke, C. Bernhardt, K. Heilig, L. A. Schaller, L. Schellenberg, E. B. Shera, and C. W. de Jager, Nuclear Ground State Charge Radii from Electromagnetic Interactions, *Atom. Data Nucl. Data Tabl.* **60**, 177 (1995).
- [37] M. Luzum, M. Hippert, and J.-Y. Ollitrault, Methods for systematic study of nuclear structure in high-energy collisions, *Eur. Phys. J. A* **59**, 110 (2023), [arXiv:2302.14026 \[nucl-th\]](#).
- [38] G. Giacalone, G. Nijs, and W. van der Schee, Determination of the Neutron Skin of Pb208 from Ultrarelativistic Nuclear Collisions, *Phys. Rev. Lett.* **131**, 202302 (2023), [arXiv:2305.00015 \[nucl-th\]](#).
- [39] A. Trzcinska, J. Jastrzebski, P. Lubinski, F. J. Hartmann, R. Schmidt, T. von Egidy, and B. Klos, Neutron density distributions deduced from anti-protonic atoms, *Phys. Rev. Lett.* **87**, 082501 (2001).
- [40] M. Abdallah et al. (STAR), Search for the chiral magnetic effect with isobar collisions at $\sqrt{s_{NN}}=200$ GeV by the STAR Collaboration at the BNL Relativistic Heavy Ion Collider, *Phys. Rev. C* **105**, 014901 (2022), [arXiv:2109.00131 \[nucl-ex\]](#).
- [41] A. Caldwell and H. Kowalski, Investigating the gluonic structure of nuclei via J/ψ scattering, *Phys. Rev. C* **81**, 025203 (2010).
- [42] X. Roca-Maza, M. Centelles, X. Vinas, and M. Warda, Neutron skin of ^{208}Pb , nuclear symmetry energy, and the parity radius experiment, *Phys. Rev. Lett.* **106**, 252501 (2011), [arXiv:1103.1762 \[nucl-th\]](#).
- [43] M. B. Tsang et al., Constraints on the symmetry energy and neutron skins from experiments and theory, *Phys. Rev. C* **86**, 015803 (2012), [arXiv:1204.0466 \[nucl-ex\]](#).
- [44] B.-A. Li, B.-J. Cai, W.-J. Xie, and N.-B. Zhang, Progress in Constraining Nuclear Symmetry Energy Using Neutron Star Observables Since GW170817, *Universe* **7**, 182 (2021), [arXiv:2105.04629 \[nucl-th\]](#).
- [45] D. Adhikari et al. (PREX), Accurate Determination of the Neutron Skin Thickness of ^{208}Pb through Parity-Violation in Electron Scattering, *Phys. Rev. Lett.* **126**, 172502 (2021), [arXiv:2102.10767 \[nucl-ex\]](#).
- [46] B. T. Reed, F. J. Fattoyev, C. J. Horowitz, and J. Piekarewicz, Implications of PREX-II on the equation of state of neutron-rich matter, *Phys. Rev. Lett.* **126**, 172503 (2021), [arXiv:2101.03193 \[nucl-th\]](#).
- [47] T. T. Chou and C.-N. Yang, Model of Elastic High-Energy Scattering, *Phys. Rev.* **170**, 1591 (1968).
- [48] L. Durand, III and R. Lipes, Diffraction model for high-energy p p scattering, *Phys. Rev. Lett.* **20**, 637 (1968).
- [49] F. Borkowski, G. G. Simon, V. H. Walther, and R. D. Wendling, On the determination of the proton RMS-radius from electron scattering data, *Z. Phys. A* **275**, 29 (1975).
- [50] X.-N. Wang and M. Gyulassy, HIJING: A Monte Carlo model for multiple jet production in p p, p A and A A collisions, *Phys. Rev. D* **44**, 3501 (1991).
- [51] M. Bahr et al., Herwig++ Physics and Manual, *Eur. Phys. J. C* **58**, 639 (2008), [arXiv:0803.0883 \[hep-ph\]](#).
- [52] D. d'Enterria and C. Loizides, Progress in the Glauber Model at Collider Energies, *Ann. Rev. Nucl. Part. Sci.* **71**, 315 (2021), [arXiv:2011.14909 \[hep-ph\]](#).
- [53] R. Abdul Khalek et al., Science Requirements and Detector Concepts for the Electron-Ion Collider: EIC Yellow Report, *Nucl. Phys. A* **1026**, 122447 (2022), [arXiv:2103.05419 \[physics.ins-det\]](#).
- [54] J.-Y. Hu, H.-j. Xu, X. Wang, and S. Pu, Probing the tetrahedral α clusters in relativistic $^{16}\text{O} + ^{16}\text{O}$ collisions, (2025), [arXiv:2507.01493 \[nucl-th\]](#).
- [55] P. Skands, S. Carrazza, and J. Rojo, Tuning PYTHIA 8.1: the Monash 2013 Tune, *Eur. Phys. J. C* **74**, 3024 (2014), [arXiv:1404.5630 \[hep-ph\]](#).
- [56] K. Hagino, H. Sagawa, J. Carbonell, and P. Schuck, Coexistence of BCS and BEC-like pair structures in halo nuclei, *Phys. Rev. Lett.* **99**, 022506 (2007), [arXiv:nucl-th/0611064](#).
- [57] Y. Kubota et al., Surface localization of the dineutron in ^{11}Li , *Phys. Rev. Lett.* **125**, 252501 (2020), [arXiv:2010.04802 \[nucl-ex\]](#).
- [58] D. D. Zhang, Z. X. Ren, P. W. Zhao, D. Vretenar, T. Nikšić, and J. Meng, Effects of rotation and valence nucleons in molecular α -chain nuclei, *Phys. Rev. C* **105**, 024322 (2022), [arXiv:2111.13437 \[nucl-th\]](#).
- [59] Q. Zhao, M. Kimura, B. Zhou, and S.-h. Shin, The universal size compression effect of nucleon pair in finite nuclei, (2025), [arXiv:2510.19280 \[nucl-th\]](#).
- [60] H. Mäntysaari and B. Schenke, Revealing proton shape fluctuations with incoherent diffraction at high energy, *Phys. Rev. D* **94**, 034042 (2016), [arXiv:1607.01711 \[hep-ph\]](#).
- [61] S. Deb, G. Sarwar, D. Thakur, P. Subramani, R. Sahoo, and J.-e. Alam, Glauber model for a small system using the anisotropic and inhomogeneous density profile of a proton, *Phys. Rev. D* **101**, 014004 (2020), [arXiv:1909.13509 \[hep-ph\]](#).